

# Dissociative recombination of $\text{CH}_5^+$ and $\text{CD}_5^+$ : Measurement of the product branching fractions and the absolute cross sections, and the breakup dynamics in the $\text{CH}_3 + \text{H} + \text{H}$ product channel

Magdalena Kamińska,<sup>1,2,\*</sup> Vitali Zhaunerchyk,<sup>2</sup> Erik Vigren,<sup>2</sup> Mathias Danielsson,<sup>2</sup> Mathias Hamberg,<sup>2</sup> Wolf D. Geppert,<sup>2</sup> Mats Larsson,<sup>2</sup> Stefan Rosén,<sup>2</sup> Richard D. Thomas,<sup>2</sup> and Jacek Semaniak<sup>1</sup>

<sup>1</sup>*Institute of Physics, Jan Kochanowski University, Świetokrzyska 15, PL-25406 Kielce, Poland*

<sup>2</sup>*Department of Physics, Albanova University Centre, Stockholm University, S-106 91 Stockholm, Sweden*

(Received 7 April 2010; published 1 June 2010)

The dissociative recombination (DR) of  $\text{CH}_5^+$  and  $\text{CD}_5^+$  has been studied at the heavy-ion storage ring CRYRING. The fragmentation dynamics of the dominant reaction channel  $\text{CH}_3 + \text{H} + \text{H}$  has been investigated using an imaging detector. The results indicate that a two-step process via the production of a  $\text{CH}_4$  intermediate, which has sufficient energy to fragment further to  $\text{CH}_3 + \text{H}$ , may play an important role. Discrepancies between the present and earlier results obtained from storage ring measurements with those from flowing afterglow experiments are addressed. Newly measured branching fractions in the DR of  $\text{CD}_5^+$  show an excellent agreement with branching fractions previously measured for  $\text{CH}_5^+$ , and the absolute DR cross sections have been also measured over an interaction energy range between  $\sim 0$  and 0.1 eV for both isotopologs.

DOI: [10.1103/PhysRevA.81.062701](https://doi.org/10.1103/PhysRevA.81.062701)

PACS number(s): 34.80.Lx, 37.20.+j, 37.10.Rs

## I. INTRODUCTION

Protonated methane,  $\text{CH}_5^+$ , is one of the most interesting nonclassical carbonium ions. It acts as a highly reactive intermediate in hydrocarbon reactions that are catalyzed by strong acids and also plays a key role in many electrophilic reactions [1]. Much time and effort have been spent in answering the fundamental question of the ion's structure and dynamics. In 1995 the group of Oka [2] published the first rotationally resolved spectrum. A subsequent spectra, obtained with the low-resolution laser-induced reaction (LIR) technique, was reported by Asvany *et al.* [3]. However, qualitative assignments of the features in the spectra have only been offered to the latter [4]. Despite the length of time which has passed since Oka's pioneering study a full description of the rotational transitions has not yet been delivered. Therefore,  $\text{CH}_5^+$  remains one of the most intriguing unresolved problems in the spectroscopy of small molecules. Additionally, after decades of investigation, it has finally been established that  $\text{CH}_5^+$  is a highly fluxional cation without a rigid structure. The potential energy surface for  $\text{CH}_5^+$  is described by 120 equivalent minima, separated by a series of low-energy saddle points [5]. The most stable equilibrium structure of  $\text{CH}_5^+$ , that is, the global minimum on the potential energy surface within the Born-Oppenheimer approximation, is an eclipsed  $C_5$  structure in which an  $\text{H}_2$  moiety is attached in an eclipsed orientation with respect to the  $\text{CH}_3^+$  moiety [6].

$\text{CH}_5^+$  plays important roles in many other areas of science, and there is an ongoing and substantial astro-chemical interest in this ion. The hydrocarbon chemistry in the interstellar medium offers a rich field for exploration. It covers many issues, beginning with the synthesis of methane and finishing with the origin of the polyatomic aromatic hydrocarbons (PAHs), some of the largest molecules found in interstellar space [7]. The presence of ionized hydrocarbons in molecular clouds and planetary atmospheres influences the

composition of these environments through ion-molecule or ion-electron reactions, as such processes contribute to the construction of more complex species. Among the many ion-electron reactions, dissociative recombination (DR) deserves a great deal of attention. For instance, the DR of  $\text{CH}_5^+$  can lead to a formation of a wide range of small reactive hydrocarbon radicals ( $\text{CH}$ ,  $\text{CH}_2$ , and  $\text{CH}_3$ ) and therefore strongly affects the molecular chemistry in the astrophysical environments in which this reaction occurs.

Dissociative recombination is a process in which a free electron is captured by a singly-charged molecular ion to form a highly excited neutral molecule, which can release the excess energy by dissociation into neutral fragments. Since DR in general possesses no energy barrier and occurs very efficiently at low interaction energies, it is a crucial reaction in cold plasmas such as molecular clouds and planetary atmospheres. Both the rate coefficients and the neutral product branching fractions are crucial information which are necessary to investigate the role of DR on the chemistry of these media. The different theoretical treatments [8–12] which are used to predict the DR branching fractions do not deliver consistent results for the same molecular systems. Due to the absence of a uniform theoretical model greater emphasis is placed on the experiment, which, in most of the cases, is the only source of relevant information.

The many experimental studies dedicated to the DR of the protonated carbocation family, that is,  $\text{CH}_n^+$ , where  $n = 1, 2, \dots, 5$ , have delivered a comprehensive data set consisting of reaction rate coefficients and branching fractions [13–18]. However, in the case of  $\text{CH}_5^+$ , the majority of the published results have only intensified the controversy around the DR of this molecule instead of shining light on the process [18–26]. In particular, results reported from two radically different experimental methods [flowing afterglow (FALP) and ion storage ring] do not converge in terms of either the rate coefficient or the branching behavior. Semaniak *et al.* [18] reported the dominance of the three-body channel  $\text{CH}_3 + \text{H} + \text{H}$  ( $\approx 70\%$ , CRYRING), while the group of Adams and co-workers observed that the  $\text{CH}_4 + \text{H}$  channel dominates

\*mkaminska@ujk.kielce.pl

( $\approx 95\%$ , FALP) [26]. Furthermore, as with the DR of  $\text{CH}_5^+$  [18], in many storage ring studies on the DR of small polyatomic, hydrogen- and deuterium-rich ions, three-body fragmentation has been observed as the dominant product channel at  $\approx 60\%$ – $80\%$  of the reaction flux [13,14,27–38].

Due to its general dominance it is reasonable to place emphasis on the three-body fragmentation channel and answer the question of whether it is a prompt or two-step process. In the latter case, the intermediate molecule formed in the initial two-body breakup process is created with sufficient internal energy that it fragments further. However, due to technical limitations, it was not generally possible to distinguish between these two possible mechanisms. The implementation of an innovative imaging detection system to DR studies at ion storage rings made it possible to investigate the fragmentation dynamics of the DR process [39,40]. Of relevance to the current study, Hellberg *et al.* [41] investigated the three-body channel in the DR of  $\text{SD}_2^+$  and showed that flux into this channel could partly arise through the predissociation of the  $\text{SD}(A^2\Sigma^+)$  state initially formed in the  $\text{SD} + \text{D}$  channel. A similar tendency had been observed earlier in the Lyman- $\alpha$  photodissociation of the neutral  $\text{SD}_2$  molecule [42,43]. Furthermore, it has recently been reported that a sequential breakup process might also be responsible for the formation of the  $\text{O}(^3P) + \text{O}(^1D) + \text{O}(^1D)$  channel in the DR of the ozone cation [44].

We recently presented a short report [45] on an investigation into the breakup dynamics of the  $\text{CH}_3 + \text{H} + \text{H}$  channel arising from the DR of  $\text{CH}_5^+$  with the aim of explaining the discrepancy between the chemical branching fractions reported from measurements made using storage rings and flowing afterglows. This investigation enabled us to conclude that the discrepancy could be due to the different pressure in these two experiments. This paper extends and expands on the results presented in the earlier short report and provides a more in-depth discussion of the data analysis and experimental details. Furthermore, we also present the latest results from CRYRING measurements on the DR rate coefficient of  $\text{CH}_5^+$  to try to address the large spread in reported values which vary by a factor of 3 [18–26]. Finally, the chemical branching fractions and rate coefficients in the DR of  $\text{CD}_5^+$  are reported to provide more insight into potential isotope effects.

## II. EXPERIMENT

The experiment has been carried out at the heavy-ion storage ring CRYRING, which is located at the Manne Siegbahn Laboratory in Stockholm, Sweden. A hollow cathode ion source JIMIS [46] was used to produce the  $\text{CH}_5^+$  and  $\text{CD}_5^+$  ions from a gas mixture of  $\text{H}_2/\text{D}_2$  and  $\text{CH}_4/\text{CD}_4$ , respectively. The ions were extracted from the source, mass selected, and injected into the ring. Ion masses of 17 amu  $^{12}\text{CH}_5^+$  and 22 amu  $^{12}\text{CD}_5^+$  were chosen in order to maximize the ion current. The ions were accelerated in the ring and stored for a few seconds prior to measurement to allow the ions to undergo vibrational relaxation.

CRYRING is a nearly circular ion storage ring, which consists of 12 straight sections. One of the sections is equipped with a so-called electron cooler, where the reactions between the ions and the electrons occur. The name originates from the effect of reducing the phase space occupied by the ions by their

interactions with the continuously renewed, cold electrons [47]. The electron beam is characterized by an anisotropic Maxwellian distribution with the transverse and longitudinal temperature components being  $kT_\perp = 2$  meV and  $kT_\parallel = 0.1$  meV, respectively:

$$f(v, v_d) = \frac{m_e}{2\pi kT_{e\perp}} \left( \frac{m_e}{2\pi kT_{e\parallel}} \right)^{1/2} \times \exp\left( -\frac{m_e v_\perp^2}{2kT_{e\perp}} - \frac{m_e (v_\parallel - v_d)^2}{2kT_{e\parallel}} \right). \quad (1)$$

The neutral products from the DR reactions occurring in the electron cooler are separated from the ion beam in the first bending magnet following the electron cooler. They leave the ring tangentially and travel to the detection area where they are detected using two different detection systems according to the aim of the measurement. In order to investigate the three-body fragmentation a position-sensitive imaging detector (ID) is used, and this is located  $\approx 7$  m from the center of the interaction region. In the cross section and the branching fraction experiments particles are detected with an ion-implanted silicon detector at the distance of  $\approx 4$  m from the center of the electron cooler.

### A. Imaging detection system

The ID consists of a stack of three microchannel plates (MCPs), a phosphor screen, and a charge coupled device (CCD) camera which has a photosensitive chip of  $64 \times 64$  pixels and a size of  $1.024 \times 1.024$  mm<sup>2</sup>. When a neutral fragment hits the first MCP it gives rise to an avalanche of secondary electrons, which is then further amplified by the following two MCPs. The electron cloud emerging from the final plate is accelerated to the phosphor screen, giving rise to a flash of light which is then projected onto the CCD chip by means of two focusing lenses. The ID is operated in a switched-off mode in which an image intensifier (II) is employed as a shutter for the CCD camera. This mode of operation implies that CCD frames are acquired at a speed of  $< 500$  Hz such that each frame contains spots originating predominantly from a single DR reaction. This enabled us to significantly reduce background contributions and to eliminate uncorrelated false-coincidence events (i.e., when one frame contains spots from independent DR reactions). This mode of operation is realized in the following way. A photomultiplier tube (PMT), which acts as a trigger for the II, is used to detect the first DR fragment on the phosphor screen. At a time 200 ns later the II is switched off for 2 ms. The time of 200 ns is sufficiently long for all of the fragments from the same DR event to reach the MCP and 2 ms corresponds to the time required for the ID software to transfer the collected data to the data-acquisition computer. During the time that the II is switched off, the PMT is vetoed to prevent retriggering.

In this mode of operation the ID functions as a two-dimensional (2D) detector. Earlier experiments [48] utilized a multianode PMT to provide arrival time information on the DR products. This 3D mode proved to be useful only for studying the DR of diatomic ions and was significantly less successful in studies of triatomic ions [39]. Furthermore,

the energy differences between adjacent rovibrational energy levels in the CH<sub>3</sub> fragments are too small to allow extraction of any useful timing information. Therefore, in the present study, only 2D data were acquired.

Since the fragments are indistinguishable in the CCD frame, a foil-tagging identification technique has been applied [39,49]. Such a technique is realized by means of a thin Al foil which is mounted in front of the first MCP. The foil is 5 mm in diameter and 2.5 μm thick such that a CH<sub>3</sub> radical has enough energy, 3.75 MeV, to pass through the foil, while hydrogen atoms with an energy of 250 keV are stopped. With respect to the center-of-mass (c.m.) frame, due to the conservation laws of momenta and energies, the heavy CH<sub>3</sub> fragment will receive only a small fraction of the available kinetic energy, which means that the CH<sub>3</sub> displacement from the c.m. is much smaller than those for hydrogen fragments. Since the CH<sub>3</sub> position on the MCP in a good approximation corresponds to the c.m. the foil was placed in the middle of the MCP so that most of the fragments hitting the foil were CH<sub>3</sub>.

### B. Ion-implanted silicon detectors

In the present experiments two ion-implanted silicon detectors with active areas of 900 and 3000 mm<sup>2</sup> were used. One advantage in using the small detector is its higher resolution. However, the larger detector usually collects all particles, even those which gain a sufficiently large transverse kick from the reaction and which miss the small detector. Therefore, the large detector was used to measure the cross sections and branching fractions for the DR of CH<sub>5</sub><sup>+</sup> while the small detector was used in the study on CD<sub>5</sub><sup>+</sup>. The output signal from the detector is proportional to the amount of kinetic energy of the incoming particles deposited in the active region of the detector. This signal after amplification with a linear amplifier is monitored by a multichannel analyzer to give a pulse-height spectrum. For measurements of the reaction cross section the DR count rate was measured by discriminating any signals with amplitude other than that corresponding to the full beam energy and recording the signal versus storage time with a multichannel scaler [36].

## III. DATA ANALYSIS

### A. Analysis of imaging data

#### 1. Monte Carlo simulation

Since 2D data are collected, only the projection of the fragment's velocities onto the surface of the first MCP has been derived. A Monte Carlo simulation (MCS) initially developed by Müller and Cosby for photodissociation studies of H<sub>3</sub> [50], and subsequently extended by Thomas *et al.* [39] to DR experiments, is employed to account for the 2D response of the ID [i.e., it provides a method to simulate all possible molecular orientations in space with respect to the detector surface and kinetic energy ( $E_k$ ) sharing among the DR fragments]. In the MCS the orientation of the molecular plane is defined by Eulerian angles ( $\phi, \theta, \psi$ ). Due to the axial symmetry of the interaction region,  $\phi$  and  $\psi$  angles are randomly distributed between 0 and  $2\pi$ . It was shown that at interaction energies  $\approx 0$  eV the DR products distribution is isotropic and in this case  $\cos\theta$  is evenly distributed between  $-1$  and  $1$  [39]. If the

molecular plane is defined, then according to the momentum and energy conservation, only two parameters are required for a complete description of fragments momenta. For instance, Müller and Cosby choose these parameters to be fractions of the total  $E_k$  received upon breakup by two of the fragments, while Thomas *et al.* in the case of  $X + H + H$  breakup used an intermolecular angle measured between two hydrogen atoms in the c.m. frame and ratios of their kinetic energies. In the present paper, for analysis we will employ these two different approaches.

The approach by Müller and Cosby was developed for homonuclear three-body breakup and here we extend its application to the nonsymmetric  $X + H + H$  fragmentation. Defining  $a, b$ , and  $c$  as the fraction of the  $E_k$  received by the CH<sub>3</sub> fragment and two hydrogen atoms, respectively ( $a + b + c = 1$ ), such that  $b < c$ , then  $a$  and  $b$  can take the following values:

$$\begin{aligned} 0 \leq a &\leq \frac{2m_H}{2m_H + m_{CH_3}}, \\ \frac{1}{2} \left[ (1-a) - \frac{1}{m_H} \sqrt{am_{CH_3}(2m_H - a(2m_H + m_{CH_3}))} \right] & \\ &\leq b \leq \frac{1}{2}(1-a). \end{aligned} \quad (2)$$

Then the components of the momenta in the plane can be defined as

$$\begin{aligned} \mathbf{u}_{CH_3} &= (u_{1x}, 0, 0), \\ \mathbf{u}_{H_1} &= (u_{2x}, u_y, 0), \\ \mathbf{u}_{H_2} &= (-(u_{1x} + u_{2x}), -u_y, 0), \end{aligned} \quad (3)$$

where

$$\begin{aligned} u_{1x} &= \sqrt{2am_{CH_3}E_k}, \\ u_{2x} &= \sqrt{2m_{CH_3}E_k} \left( \frac{m_H - a(m_{CH_3} + m_H) - 2bm_H}{2m_{CH_3}\sqrt{a}} \right), \\ u_y &= \sqrt{2m_H E_k} \left[ b - \left( \frac{m_H - a(m_{CH_3} + m_H) - 2bm_H}{2\sqrt{am_{CH_3}m_H}} \right)^2 \right]^{\frac{1}{2}}. \end{aligned} \quad (4)$$

The hydrogen fragments were assigned according to their energies as  $E_{H_1} < E_{H_2}$ .

#### 2. Investigation into the reaction energy distribution

The displacement of each fragment from the c.m.,  $d_{cm}$ , was measured for every CCD frame containing three spots, such that the spot at the position corresponding to the foil was assigned to the CH<sub>3</sub> fragment and the two others to the hydrogen atoms. It is noted that the CCD frames with only one spot behind the foil were accepted for the analysis. The displacement of the fragments is related to  $E_k$  (i.e., the higher the energy the larger the separation of the spots). The total displacement,  $T_D$ , is defined as

$$T_D = \left( \frac{m_{CH_3}}{m_H} d_{cm-CH_3}^2 + d_{cm-H_1}^2 + d_{cm-H_2}^2 \right)^{\frac{1}{2}} \quad (5)$$

and is directly proportional to  $\sqrt{E_k}$  and, therefore, can be used to find the  $E_k$  distribution. The experimentally measured

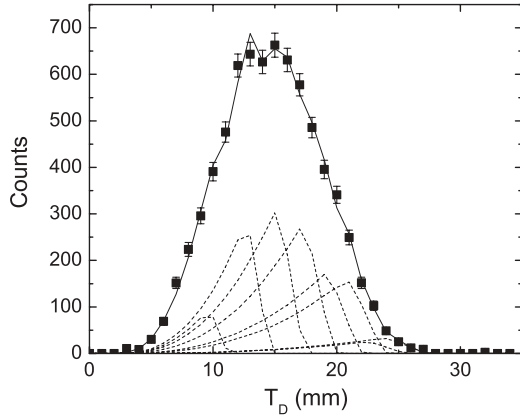


FIG. 1. The experimentally measured  $T_D$  distribution corrected for background signals is shown by the solid squares with purely statistical error bars. The MCS results are depicted by the dotted curves and the overall fit is shown by the solid black curve.

$T_D$  distribution is shown in Fig. 1 by the solid squares and is corrected for contributions from background signals. The background elimination was performed by determining the  $T_D$  distribution for fragments detected at an interaction energy of 1 eV where background signals completely dominate over DR events and this distribution was subtracted from that measured at  $\approx 0$  eV. The background contribution was estimated to be  $\approx 15\%$ . Using the three velocity components of the fragments measured in each CCD frame, the range of  $T_D$  values is determined by

$$T_D = \sqrt{\frac{E_k}{m_H} \frac{m_i}{E_{\text{beam}}}} L', \quad (6)$$

where  $L'$  is the distance from where the DR reaction occurs to the detector and  $L - l/2 \leq L' \leq L + l/2$ , where  $L$  is the distance from the middle of the electron cooler to the detector and  $l$  is the length of the interaction region.  $E_{\text{beam}}$  is the energy of the ion beam. However, since the ID only measured the projection of the fragments' velocity, the  $T_D$  distribution is significantly broadened. To the best of our knowledge, analytical expressions do not exist to provide a general description of such three-particle distributions and the MCS was implemented to calculate these.

The exothermicity of the  $\text{CH}_3 + \text{H} + \text{H}$  channel is insufficient to create electronically excited fragments and the available kinetic energy can only be diminished through rovibrational excitation of the  $\text{CH}_3$  radicals [45]. As such, the experimentally measured  $T_D$  distribution represents an overlap of the contributions from various rovibrational states. However, the resolution of the detector does not allow a detailed investigation of these states. It is noted that so far it has only been feasible to resolve contributions from the electronic states [35,39,41,49,52] although, quite recently, it has been demonstrated for the  $\text{OH}(v = 0-2)$  states arising from the DR of  $\text{H}_3\text{O}^+$  [53]. In order to estimate the reaction energy distribution, MCS-generated  $T_D$  distributions for  $E_k$  values ranging from 0.15 to 3.35 eV with a step of 0.4 eV (Fig. 1, the dotted curves) have been created. These distributions were then fitted to the experimental data and the fitting coefficients

used to determine the contributions from each particular  $E_k$  value.

### 3. Investigation into the breakup dynamics

An investigation into the breakup dynamics was performed using an approach similar to that described in Refs. [39,54]. In order to find an actual distribution of the parameters describing breakup dynamics, such as breakup geometries or  $E_k$  sharing among the fragments, the experimentally measured distribution should be divided by that generated by an MCS in which the fragmentation is completely isotropic in the molecular frame. This method was first suggested for the DR three-body breakup of  $\text{H}_3^+$  in which information about breakup geometries was investigated by means of a Dalitz plot [54]. In particular, it was found that linear breakup geometries are overestimated in the detector plane, since any breakup geometry can be oriented in space such that its projection will be linear. Subsequently, Thomas *et al.* [39] investigated in a similar way breakup angles of the water molecules undergoing DR reactions and proved this method to be valid in this case as well. Similar to conclusions drawn from a Dalitz plot [54], it was also found that intermolecular linear angles (i.e., when the angle measured between H atoms in their c.m. frame is either close to 0 or 180 degrees) dominate in the detector plane when the initial angular distribution is random in space.

When the breakup dynamics are investigated by means of the  $E_k$  fractions received by two hydrogen atoms, these values are found from experimental measurements as

$$E_{\text{H}_1} = \frac{d_{\text{cm-H}_1}^2}{T_D^2}, \quad E_{\text{H}_2} = \frac{d_{\text{cm-H}_2}^2}{T_D^2}. \quad (7)$$

The distributions of these parameters generated by the MCS in the detector plane, for fully randomized parameters, are shown in Fig. 2(a) by the dashed curves. For investigation into the breakup dynamics, three-body events with  $T_D > 20$  mm were analyzed first, for which  $E_k$  cannot be smaller than 2 eV. The distributions derived from the experimental data with these  $T_D$  values are presented in Fig. 2(a), and the estimated distribution in the molecular frame [i.e., the experimental distribution divided by that shown in Fig. 2(a) by the dashed curves] is depicted in Fig. 2(d).

In the next step we studied the breakup dynamics for the three-body events with  $T_D$  values smaller than 20 mm. This analysis can provide important insight into any dependence of the breakup dynamics on the rovibrational excitation of the  $\text{CH}_3$  fragments. The experimentally measured  $E_{\text{H}_1}$  and  $E_{\text{H}_2}$  distributions for events with  $14 < T_D < 20$  and  $T_D < 14$  mm are presented in Figs. 2(b) and 2(c), respectively, and the corresponding distributions in the molecular frame derived by means of MCS are shown in Figs. 2(e) and 2(f), respectively.

The data with  $T_D > 20$  mm were also analyzed via a parameter  $\rho$  which describes the ratio between hydrogen atom energies, that is,  $\rho = (d_{\text{cm-H}_1}/d_{\text{cm-H}_2})^2$  [35,39,41,49]. The experimental and the Monte Carlo simulated distributions are shown in Fig. 3(a) by the solid squares and the dotted curves, respectively, and the ratio is presented in Fig. 3(b).

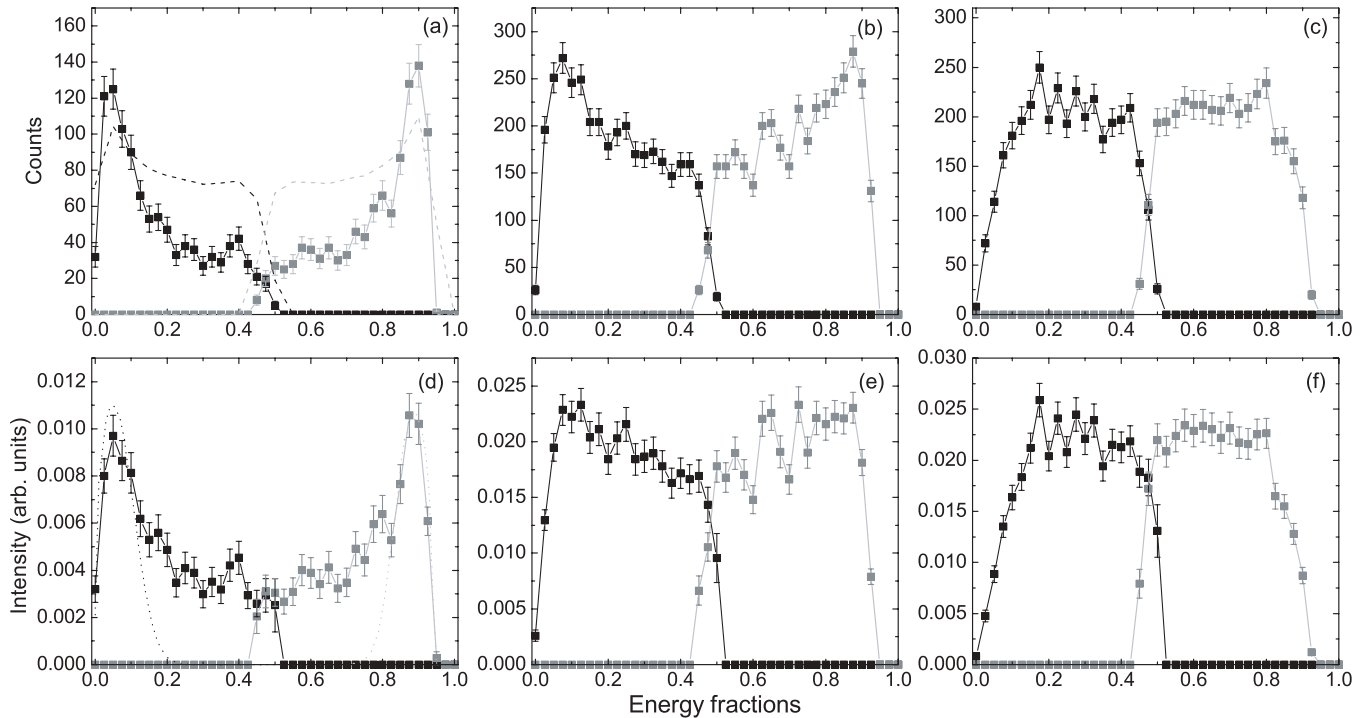


FIG. 2. The fraction of the  $E_k$  received by the H<sub>1</sub> and H<sub>2</sub> atoms in the CH<sub>3</sub> + H + H channel are shown in black and gray, respectively. In (a), (b), and (c) the experimentally measured distributions obtained for the three-body events with  $T_D > 20$ ,  $14 < T_D < 20$ , and  $T_D < 14$  mm, respectively, are shown by the solid squares and the corresponding distributions derived in the molecular frame by means of the MCS are plotted as solid squares in (d), (e), and (f), respectively. The dotted curve in (a) shows the MCS generated distributions obtained in the detector plane when the parameters  $a$  and  $b$  are evenly distributed in the molecular frame. The results obtained from the free-rotator model [51] are plotted in (d) by the dotted line. The error bars correspond to statistical uncertainties.

### B. Cross section

The DR cross section as a function of the interaction energy between the electrons and the ions was also investigated. The kinetic energy of the electrons,  $E_e$ , is given by the

electron cathode gun voltage and this can be changed in a controlled manner during the experiment. During the ramping of this voltage, at every time step the collision energy, or detuning energy, is well defined and is given by the equation

$$\sqrt{E_d} = \sqrt{E_e} - \sqrt{E_{\text{cool}}}, \quad (8)$$

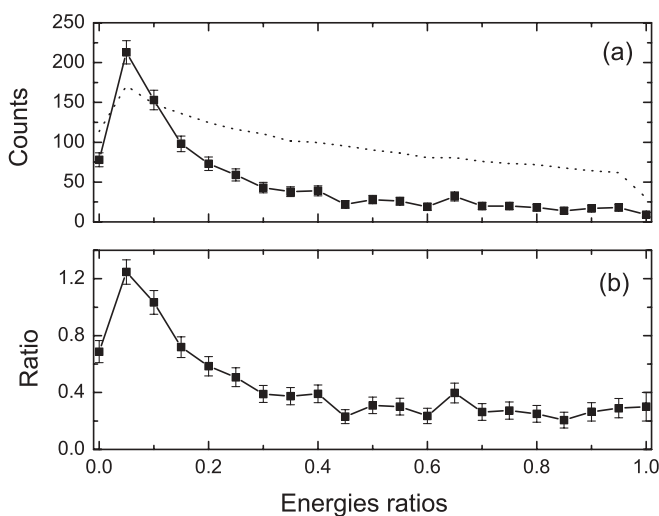


FIG. 3. (a) The  $\rho$  distributions obtained for three-body events with  $T_D > 20$  mm are shown by the solid squares and the corresponding distribution obtained with the MCS when  $\rho$  was evenly distributed between 0 and 1. (b) The ratio of distributions from (a).

where  $E_{\text{cool}}$  is the cooling energy corresponding to the kinetic energy of the electrons when they move with the same average velocity as the ions. The energies  $E_e$  and  $E_{\text{cool}}$  are corrected for the space charge effect induced by the electrons [55] and partial neutralization of this effect by trapped positive ions arising from the ionization of rest-gas particles [18].

Figure 4(a) shows the scheme used to ramp the electron cathode voltage to cover the interaction energy region from 1 to 0 eV. During each cycle after injection, acceleration, and cooling of the ions, the velocity of the electrons is changed such that they move faster than the ions, then they slow down to end up moving slower than the ions. The pure DR spectrum measured with the ion-implanted silicon detector after subtraction of the background events originating from collisions with the residual gas is presented in Fig. 4(b). The decay of the ion beam is monitored by a separate MCP detector located in one of the straight sections of the ring. The detector counts the number of neutral particles which originate from

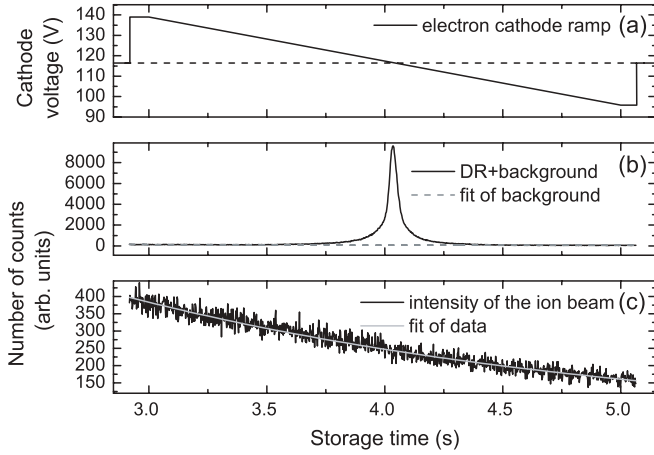


FIG. 4. (a) Cathode voltage vs storage time during cross section measurement for  $\text{CD}_5^+$ . (b) The pure DR signal obtained after the subtraction of background recorded with a multichannel scaler. (c) The decay of the ion beam monitored by the MCP detector.

reactions between the ions and the rest-gas molecules present in the ring as a function of storage time. The neutral particle spectrum is therefore proportional to the number of ions in the beam. Figure 4(c) shows the spectrum measured with the MCP detector.

The measured DR rate coefficient  $\alpha(E_d)$ , which is the velocity-weighted cross section averaged over the electron velocity distribution in the electron beam, was determined from the equation

$$\alpha(E_d) = \frac{dN_{\text{DR}}}{dt} \frac{v_e v_i e^2 r_e^2 \pi}{I_e I_i l}, \quad (9)$$

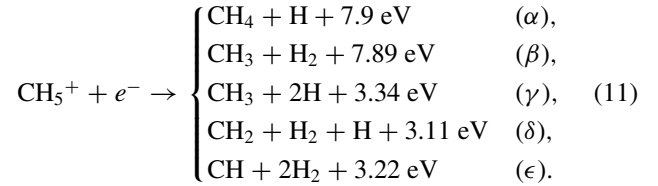
where  $dN_{\text{DR}}/dt$  is the count rate of DR events,  $e$  is the elementary charge,  $v_e$  and  $v_i$  are electron and ion velocities in the laboratory frame of reference, respectively,  $l$  is the length of the parallel interaction region in the electron cooler,  $r_e$  and  $I_e$  are the radius and the current of the electron beam, and  $I_i$  is the ion-beam current, which at CRYRING can be precisely measured down to 0.1 nA [56,57].

The absolute cross section is obtained after deconvolution from the measured rate coefficient and correcting for the so-called toroidal effect [58]. For collision energies lower than the energy spread of the electrons, the formula  $\sigma(E) = \alpha(E_d)/v_d$ , where  $v_d = \sqrt{2E_d/m_e}$ , is no longer valid and a numerical Fourier transform technique [59] is implemented to evaluate the cross section. The thermal rate coefficient as a function of the electron temperature  $T$  is calculated by integrating the absolute cross section  $\sigma(E)$  over the electron energy distribution under thermal equilibrium conditions:

$$\alpha(T) = \frac{8\pi m_e}{(2\pi m_e kT)^{3/2}} \int_0^\infty E \sigma(E) e^{-E/kT} dE. \quad (10)$$

### C. Product branching fractions

In the DR of  $\text{CH}_5^+$  ions with near-zero-eV electrons the following channels are energetically accessible:



The kinetic energy releases listed here are calculated by assuming that the products and the parent ion are in their vibronic ground states. Since the isotopic shift for the deuterated species is not significant, the quoted energies will be the same for the respective channels in the DR of  $\text{CD}_5^+$ . The neutral fragments from one DR event reach the detector within a very short time interval. The shaping time of the detector amplifier is much longer and so the neutral products are detected as one event and the pulse-height spectrum of the output signal from the detector amplifier consists of only one peak at the position corresponding to the kinetic energy of the parent ion. A typical energy spectra measured with the electron beam energy tuned to collision energies of  $\approx 0$  and 1 eV are shown in Figs. 5(a) and 5(b), respectively. Note that the scale on the left-hand side in Fig. 5(a) is much smaller than that on the right-hand side.

In order to determine the product branching fractions a grid with a transmission of  $t = 0.297 \pm 0.015$  [36] was inserted in front of the ion-implanted silicon detector. Figures 6(a) and 6(b) show the typical neutral product pulse-height energy spectra measured with the grid in front of the detector at  $\approx 0$  and 1 eV collision energy, respectively. Particles can pass through the grid (which is made of stainless steel, 50  $\mu\text{m}$  thick, with holes of  $\approx 80 \mu\text{m}$  diameter); otherwise they are stopped and are not measured. Consequently, the pulse-height spectrum of the DR products with the grid in front of the detector is no longer a single peak at the position corresponding to the full ion beam energy. Instead it consists of a series of peaks at different positions defined by the energy carried by those fragments which are detected. Each fragment with a

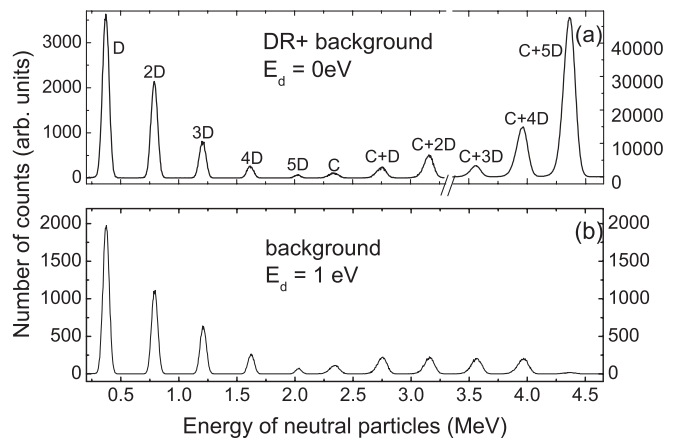


FIG. 5. Energy spectra of neutral fragments from DR of  $\text{CD}_5^+$  measured without the grid in front of the detector. (a) The spectrum measured with a detuning energy of 0 eV. (b) Background spectrum collected after changing the detuning energy to 1 eV.

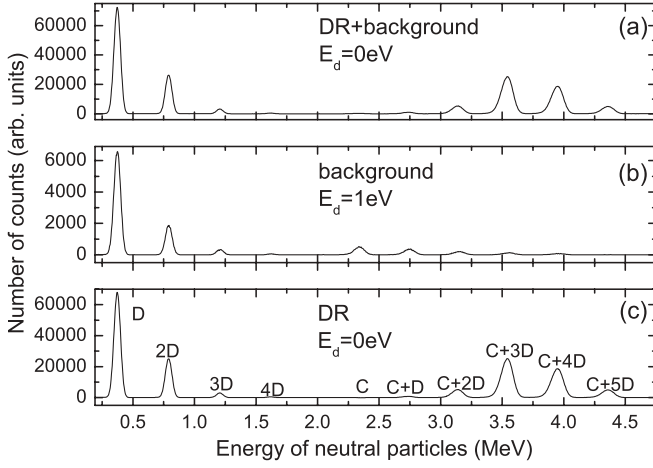


FIG. 6. Energy spectra of neutral fragments from DR of CD<sub>5</sub><sup>+</sup> measured with the grid in front of the detector. (a) The spectrum measured with the detuning energy of 0 eV. (b) Background spectrum collected after changing the detuning energy to 1 eV. (c) The pure DR spectrum obtained after the subtraction of the background.

mass of  $M_x$  carries a fraction of the full beam energy  $E_{\text{beam}}$  given by  $E_{\text{beam}}M_x/M_{\text{beam}}$ , where  $M_{\text{beam}}$  is the mass of the ion. Therefore, the particular peaks in the spectrum can be attributed to the fragments with mass  $M_x$ , and this is illustrated in Figs. 5(a) and 6(c).

The spectra recorded with the electron beam energy tuned to a collision energy of 0 eV [Figs. 5(a) and 6(a)] contains signals which also originate from background processes, such as charge transfer reactions between the ions and the residual gas in the electron cooler. These background contributions are subtracted from the DR signal by making use of the spectra measured at 1 eV collision energy [Figs. 5(b) and 6(b)], which were assumed to be dominated by background events (since the DR cross section at this energy is vanishingly small) and the ion beam intensity spectra monitored with the MCP detector were used for normalization. Spectra at 1 and 0 eV collision

energy after being normalized to the intensity of the ion beam measured with the MCP detector were subtracted from each other, thus yielding a neutral product pulse-height distribution spectrum [Fig. 6(c)] arising purely from DR reactions.

The intensities of the peaks can be expressed in terms of the product branching fractions, the transmission probability, and the loss factors. The probability for a particle to be stopped by the grid or pass through is  $1 - t$  or  $t$ , respectively. For example, neutral DR products produced in dissociation channel  $\alpha$  can be detected either with the total ion beam energy with a probability of  $t^2$ , or with the energy carried by the CD<sub>4</sub> fragment with a probability of  $t(1 - t)$ , or with the energy carried by the D fragment with the same probability  $t(1 - t)$ . Loss factors are the correction factors included to take into account the situation when the maximum transversal separations of some of the light products in the reaction can be larger than the active area of the detector and so may miss the detector. Therefore, five correction factors  $L_\alpha$  to  $L_\epsilon$  for channels  $\alpha$  to  $\epsilon$ , respectively, representing probabilities that one of the light fragment (the D atom in case of  $L_\delta$ ) can miss the detector, were implemented. With these factors the intensities of the peaks in the pulse-height spectrum can be described by the set of Eq. (12) expressed as mentioned in terms of the grid transmission,  $t$ , and the number of events in individual dissociation channels,  $N_\alpha$  to  $N_\epsilon$ :

$$\begin{pmatrix} I_D \\ I_{2D} \\ I_{3D} \\ I_{4D} \\ I_{C+D} \\ I_{C+2D} \\ I_{C+3D} \\ I_{C+4D} \\ I_{C+5D} \end{pmatrix} = T_{\text{CD}_5^+} \times \begin{pmatrix} N_\alpha \\ N_\beta \\ N_\gamma \\ N_\delta \\ N_\epsilon \end{pmatrix}, \quad (12)$$

where the matrix  $T_{\text{CD}_5^+}$  is given as

$$\begin{pmatrix} t(1-t)L_\alpha^* & 0 & 2t(1-t)^2L_\gamma^* + t(1-t)L_\gamma & t(1-t)^2L_\delta^* & 0 \\ 0 & t(1-t)L_\beta^* & t^2(1-t)L_\gamma^* & t(1-t)^2L_\delta^* + t(1-t)L_\delta & 2t(1-t)^2L_\epsilon^* + t(1-t)L_\epsilon \\ 0 & 0 & 0 & t^2(1-t)L_\delta^* & 0 \\ 0 & 0 & 0 & 0 & t^2(1-t)L_\epsilon^* \\ 0 & 0 & 0 & 0 & t(1-t)^2L_\epsilon^* + t(1-t)L_\epsilon \\ 0 & 0 & 0 & t(1-t)^2L_\delta^* + t(1-t)L_\delta & 0 \\ 0 & t(1-t)L_\beta^* + tL_\beta & t(1-t)^2L_\gamma^* + t(1-t)L_\gamma & t^2(1-t)L_\delta^* & 2t^2(1-t)L_\epsilon^* + t^2L_\epsilon \\ t(1-t)L_\alpha^* + tL_\alpha & 0 & 2t^2(1-t)L_\gamma^* + t^2L_\gamma & t^2(1-t)L_\delta^* + t^2L_\delta & 0 \\ t^2L_\alpha^* & t^2L_\beta^* & t^3L_\gamma^* & t^3L_\delta^* & t^3L_\epsilon^* \end{pmatrix} \quad (13)$$

and  $L_\alpha^* = 1 - L_\alpha$ ,  $L_\beta^* = 1 - L_\beta$ , etc.

TABLE I.  $T_D$  distributions generated by the MCS for different  $E_K$  steps.

| $E_K$ (eV) | Contribution (%) |
|------------|------------------|
| 0.15       | 0                |
| 0.55       | 4                |
| 0.95       | 16               |
| 1.35       | 21               |
| 1.75       | 22               |
| 2.15       | 15               |
| 2.55       | 15               |
| 2.95       | 3                |
| 3.35       | 4                |

Using a least-squares fitting method the number of events,  $N_\alpha$  to  $N_\epsilon$ , and the loss factors can be found. Losses are determined to be at the level of 0.042–0.228. The branching fractions for an individual dissociation channel are finally obtained after the normalization:

$$\alpha, \beta, \gamma, \delta, \epsilon = \frac{N_{\alpha, \beta, \gamma, \delta, \epsilon}}{N_\alpha + N_\beta + N_\gamma + N_\delta + N_\epsilon}. \quad (14)$$

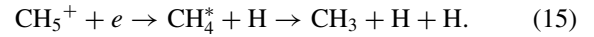
#### IV. RESULTS AND DISCUSSION

The results obtained from fitting the  $T_D$  distributions generated by the MCS, for  $E_k$  values ranging from 0.1 to 3.35 eV with a step of 0.4 eV, to the experimentally derived distribution are shown in Table I. It is noted that due to the resolution of the detection system, these results must be regarded only as a rough estimate. Nevertheless, analysis indicates that  $\text{CH}_3$  fragments are produced preferentially in rovibrationally excited states with an excess energy of 1–2.5 eV.

The  $E_{\text{H}_1}$  and  $E_{\text{H}_2}$  distributions imply that one of the hydrogen fragments receives a minute amount of  $E_k$ , while the second receives a major fraction [Fig. 2(d)]. A similar tendency is also observed from the distribution of parameter  $\rho$ , which has a peak at  $\approx 0.1$  [Fig. 3(b)]. The distributions obtained from the events with  $T_D < 20$  mm show that  $E_k$  is almost randomly shared between the fragments [Figs. 2(e) and 2(f)]. These observations can be explained in the following way. Irrespective of the internal energy contained in the  $\text{CH}_3$  radicals, the hydrogen atoms will receive  $\approx 10$  and 90% of the  $E_K$ , respectively. However, at lower  $E_k$ , the hydrogen with a smaller energy will not manage to avoid the foil and, thus, this event will not be accepted for the analysis, since it produces only two flashes on the PS. In order to support such an assertion, in the MCS  $\rho$  was assumed to be  $\approx 0.1$  and it was found that for  $E_k$  values of 2.0, 1.0, and 0.5 eV,  $\approx 33\%$ , 41%, and 60% of the three-body events would not be detected, respectively.

Based on the kinetic energy sharing between the hydrogen fragments it is possible to establish a possible dissociation route. Maul and Gericke in their review paper of the molecular three-body breakup distinguished several different dissociation mechanisms, and one such process is termed sequential [60]. In the case of the  $\text{CH}_3 + \text{H} + \text{H}$  channel this

can be described by



Here, the production of  $\text{CH}_4^* + \text{H}$  would be the first step in this process such that the intermediate  $\text{CH}_4^*$  molecule is created in a highly excited state, which subsequently decays into  $\text{CH}_3 + \text{H}$ . The kinetic energy of the hydrogen atom ejected at the first step relates to the internal excitation of the intermediate  $\text{CH}_4$  and its maximum value of  $M_{\text{CH}_4}/M_{\text{CH}_5} E_k$  corresponds to the case when internal energy of  $\text{CH}_4$  is comparable to the dissociation energy into  $\text{CH}_3 + \text{H}$ . If the intermediate molecule remains intact for a time longer than  $10^{-11}$  s, (i.e., for longer than a rotational period), the second bond rupture will be independent of the first [60]. During this time the free hydrogen atom will move a sufficient distance away from the  $\text{CH}_4$  molecule, preventing any interaction between them. Upon the second bond rupture, the second hydrogen atom will receive the major part of the remaining energy due to the ratio of  $M_{\text{CH}_3}/M_{\text{CH}_4}$ . In order to justify a stepwise process, we utilized the free-rotator model which has been successfully used to describe purely sequential breakup mechanisms [51]. Hishikawa *et al.* employed this model to study the internal excitation of intermediate species formed in the sequential breakup of molecules which had been excited by an intense fs laser [51]. If we assume that the  $E_{\text{H}_2}$  distribution of the hydrogen atom that is ejected first corresponds to that presented in Fig. 2(d) by the gray dotted curve, then according to the free-rotator model the energy distribution of the hydrogen atom produced by the second bond rupture will be described by the dotted black curve shown in Fig. 2(d). The free-rotator model reproduces the experimentally observed peak in the  $E_{\text{H}_1}$  distribution, which enables us to conclude that the three-body DR  $\text{CH}_3 + \text{H} + \text{H}$  channel can indeed proceed via a sequential decay mechanism.

The absolute cross sections for the DR of  $\text{CH}_5^+$  and  $\text{CD}_5^+$  were measured over the energy range  $\approx 0$  to 0.1 eV. Figure 7 shows the measured cross section for the DR of  $\text{CD}_5^+$  and  $\text{CH}_5^+$  after 2 and 2.2 s of cooling time, respectively. For the DR of  $\text{CH}_5^+$  the cross section was measured after four different

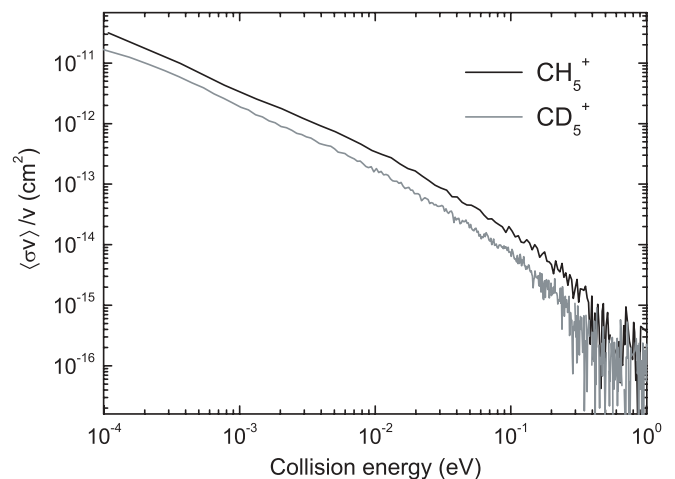


FIG. 7. Measured cross section for dissociative recombination for  $\text{CH}_5^+$  and  $\text{CD}_5^+$  as a function of collision energy.

TABLE II. DR cross sections for CH<sub>5</sub><sup>+</sup> and CD<sub>5</sub><sup>+</sup> and the following cooling times.

| Cooling time (s)             | $\sigma(E)$ (cm <sup>2</sup> )                       |
|------------------------------|--|
| CH <sub>5</sub> <sup>+</sup> |  |
| 0.5                          | $(1.63 \pm 0.09) \times 10^{-15} E^{-1.13 \pm 0.03}$ |
| 2.2                          | $(1.39 \pm 0.07) \times 10^{-15} E^{-1.19 \pm 0.03}$ |
| 4.8                          | $(1.05 \pm 0.06) \times 10^{-15} E^{-1.19 \pm 0.03}$ |
| 10.8                         | $(1.21 \pm 0.07) \times 10^{-15} E^{-1.18 \pm 0.04}$ |
| CD <sub>5</sub> <sup>+</sup> |  |
| 2s                           | $(4.2 \pm 0.11) \times 10^{-16} E^{-1.31 \pm 0.04}$  |

cooling times, and the results of the best fits of the experimental data fitted over the energy range 1–100 meV are presented in Table II. Analysis indicates that the cross section showed no evident time dependence.

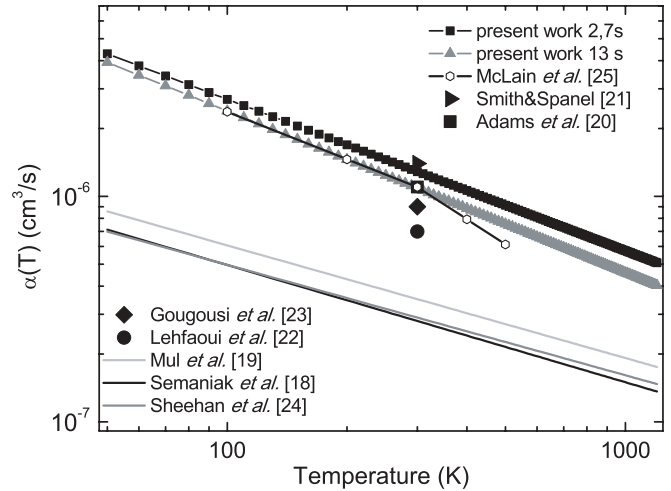
The derived energy dependence  $E^{-1.13}$ – $E^{-1.19}$  is a little bit steeper than the  $E^{-1}$  behavior expected for the direct DR mechanism according to the Wigner threshold law [61]. This result implies that the indirect process, in which the electron is resonantly captured into Rydberg states which converge to the ionic ground state before coupling to the repulsive dissociative state, plays an important role in the DR of CH<sub>5</sub><sup>+</sup> at low energies.

From the measured cross sections the thermal rate coefficients have been derived and the results of the fits over the temperature range of 50–1000 K are presented in Table III. The temperature dependencies of the rate coefficient are steeper than the theoretical value of  $T^{-0.5}$  predicted by the direct mechanism [62]. The full systematic investigation of the DR of CH<sub>5</sub><sup>+</sup> at CRYRING was previously reported by Semaniak *et al.* [18]. The thermal rate coefficient obtained from that experiment was found to be the following:  $2.8 \times 10^{-7}$  cm<sup>3</sup> s<sup>-1</sup> at 300 K; this value is barely one-third those reported in the present work for CH<sub>5</sub><sup>+</sup>. Table IV also lists the previously published data arranged in two columns. The rate coefficients are consistent in the range of  $2.7 \times 10^{-7}$  to  $3.5 \times 10^{-7}$  cm<sup>3</sup> s<sup>-1</sup> at 300 K and  $0.7 \times 10^{-6}$  to  $1.4 \times 10^{-6}$  cm<sup>3</sup> s<sup>-1</sup> at 300 K in the left and the right columns, respectively. These results are also shown in Fig. 8.

Analysis of the current results show that the thermal rate coefficient for the DR of CD<sub>5</sub><sup>+</sup> is smaller than those reported here for CH<sub>5</sub><sup>+</sup> (Table III). A similar tendency for a smaller rate coefficient for deuterated species has been observed in previous DR studies (see, e.g., H<sub>3</sub>O<sup>+</sup> vs D<sub>3</sub>O<sup>+</sup> [36], H<sub>2</sub>O<sup>+</sup>

TABLE III. Thermal rate coefficients for CH<sub>5</sub><sup>+</sup> and CD<sub>5</sub><sup>+</sup> after the following cooling times.

| Cooling time (s)             | $\alpha(T)$ (cm <sup>3</sup> s <sup>-1</sup> )            |
|------------------------------|---|
| CH <sub>5</sub> <sup>+</sup> |   |
| 0.5                          | $(1.2 \pm 0.06) \times 10^{-6} (T/300)^{-0.65 \pm 0.02}$  |
| 2.2                          | $(1.3 \pm 0.09) \times 10^{-6} (T/300)^{-0.71 \pm 0.03}$  |
| 4.8                          | $(1.01 \pm 0.06) \times 10^{-6} (T/300)^{-0.71 \pm 0.03}$ |
| 10.8                         | $(1.09 \pm 0.06) \times 10^{-6} (T/300)^{-0.72 \pm 0.03}$ |
| CD <sub>5</sub> <sup>+</sup> |   |
| 2s                           | $(7.7 \pm 0.9) \times 10^{-7} (T/300)^{-0.77 \pm 0.03}$   |

FIG. 8. Thermal rate coefficient for dissociative recombination of CH<sub>5</sub><sup>+</sup> as a function of electron temperature. Results of the previous experiments measured with FALP and with single- and multipass merged beam techniques are also presented on the plot.

versus HDO<sup>+</sup> [63], and NH<sub>4</sub><sup>+</sup> versus ND<sub>4</sub><sup>+</sup> [38]). For these ions the rate coefficient at 300 K for the deuterated isotopolog was barely one-half that of the hydrogenated isotopolog. A ratio of  $\approx 0.54$ – $0.7$  is determined for the rates of CD<sub>5</sub><sup>+</sup> and CH<sub>5</sub><sup>+</sup> reported here, similar to the other observations of this effect.

The branching fractions in the DR of CD<sub>5</sub><sup>+</sup> derived from the measured data are presented in Table V and are in good agreement within error bars with earlier CH<sub>5</sub><sup>+</sup> results obtained at CRYRING [18].

As mentioned earlier the rate coefficient for the DR of CH<sub>5</sub><sup>+</sup> reported in 1998 [18] is lower than that presented in this work by a factor of 3. There are two key differences between the two CRYRING experiments, one involving the ion source and the other the ion-current measurement. The Nielsen-type ion source used in the earlier experiment in 1998 is known to produce hotter ions compared to the hollow cathode source used in the current experiment, where the higher pressure inside the source allows efficient collisional quenching of the ions before they are extracted from the source. The different sources would give rise to different rovibronic populations of the ion beam, with the colder source producing a cooler distribution. However, it is not certain whether there exists sufficiently long lived rovibrational states which might survive after a few seconds of cooling to play a role in the measurement.

A recently installed ac current transformer allows ion-beam currents down to 0.1 nA to be measured [57], while the old dc transformer required much higher ion currents at the level of microamperes. The uncertainties of the current measurement quoted by Semaniak *et al.* are on the level of 25%. However, the possibility that this measurement was much worse than believed at that time cannot be excluded. In the recent CRYRING measurement this uncertainty was estimated to be 10%, 5%, and less than 1% for the cooling times of 0.5, 2.2, 4.8, and 10.8 s, respectively.

TABLE IV. Measured thermal rate coefficients  $\alpha = a(T/300)$  at 300 K for DR of  $\text{CH}_5^+$ .

| $\alpha(T)$<br>( $\text{cm}^3 \text{ s}^{-1}$ ) | Ref. | Method  | $\alpha(T)$<br>( $\text{cm}^3 \text{ s}^{-1}$ ) | Ref.         | Method  |
|---|------|---------|---|--------------|---------|
| $3.5 \times 10^{-7}$                            | [19] | MEIBE   | $1.1 \times 10^{-6}$                            | [20]         | FALP    |
| $2.8 \times 10^{-7}$                            | [18] | CRYRING | $1.4 \times 10^{-6}$                            | [21]         | FALP    |
| $2.7 \times 10^{-7}$                            | [24] | MEIBE   | $0.7 \times 10^{-6}$                            | [22]         | FALP    |
|   |      |         | $0.9 \times 10^{-6}$                            | [23]         | FALP    |
|   |      |         | $1.1 \times 10^{-6}$                            | [25]         | FALP    |
|   |      |         | $(1.01\text{--}1.3) \times 10^{-6}$             | present data | CRYRING |

A single pass study on the DR of  $\text{CH}_5^+$  [24] performed at the MEIBE apparatus at the University of Western Ontario, Canada, reported a rate coefficient that was quantitatively similar to the first CRYRING rate coefficient. However, FALP experiments [20,21,25] have yielded a 300-K DR rate coefficient that is in good agreement with the value that we report here. Based on the data listed in Table IV one can assume that different ion rovibrational populations were populated in the different experiments. Sheenan and St.-Maurice [24] discussed the possibility of vibrational excitation of  $\text{CH}_5^+$  ions in single- and multipass merged beam approaches as a source of the discrepancy with results from the FALP apparatus. It is likely that the electronic and vibrational ground states are easily accessible in the FALP experiment. However, due to the nonzero dipole moment [64],  $\text{CH}_5^+$  stored in CRYRING should reach its vibrational ground state within a few seconds by means of spontaneous IR emission. Furthermore, rotational cooling is also expected to be very efficient, as demonstrated in (Test Storage Ring, Heidelberg, Germany) experiments on the DR of  $\text{H}_3^+$  and its isotopologs, in which  $\text{D}_2\text{H}^+$  and  $\text{H}_2\text{D}^+$  were observed to rotationally cool while  $\text{H}_3^+$  and  $\text{D}_3^+$  retained a high rotational temperature even after 40 s of storage [65].

The branching fractions in the DR of  $\text{CD}_5^+$  and  $\text{CH}_5^+$  measured at CRYRING do not agree with the most recent FALP measurements (last column in Table V) [26]. A new technique has recently been implemented in a FALP machine in order to quantify the neutral products originating from a DR reaction. The development of this technique was motivated by the need to resolve the contradictions in branching fractions obtained from both techniques. An elaborate and detailed analysis of possible sources of errors at FALP experiments

has been undertaken, accompanied with the modeling of all eventual losses of the DR neutral products through ion-neutral recombination, neutral-neutral reactions, and the diffusive loss of neutrals. However, within this model, the most optimistic enhancement in the production of  $\text{CH}_3$  would be only by  $\approx 2\%$ , and that is still too small to explain the existing discrepancies.

The evidence for a sequential breakup mechanism suggested in this paper could serve as a crucial hint for resolving these discrepancies. Survival of the excited  $\text{CH}_4^*$  long enough to be able to fragment further depends on the prevailing conditions immediately after its formation. The ultrahigh-vacuum conditions ( $< 10^{-11}$  Torr) present in CRYRING means that DR neutral products leave the interaction region and travel to the detectors in less than  $\approx 10^{-6}$  s with almost no collisions with the residual gas molecules. However, in a FALP apparatus, the relatively high He pressure inside the flow tube,  $\approx 1$  Torr, would mean that excited molecules could be collisionally quenched at a rate of  $\approx 3 \times 10^7$  Hz, giving  $\approx 0.3 \times 10^{-7}$  s between collisions. The lifetime of the  $\text{CH}_4^*$  must be then at least longer than one rotational period of the molecule (i.e.,  $\geq 10^{-11}$  s) to fulfill the condition for the sequential breakup. Consequently, the fragmentation lifetime of excited  $\text{CH}_4$  should be longer than  $\approx 30$  ns and shorter than  $\approx 1 \mu\text{s}$  [45].

A systematic investigation into the DR of protonated methane has been undertaken and the results have been presented here. Analysis of the breakup dynamics in the fragmentation channel  $\text{CH}_3 + \text{H} + \text{H}$  reveals strong evidence for a sequential breakup mechanism via the production of  $\text{CH}_4^* + \text{H}$ . Only moderate rovibrational excitation of the  $\text{CH}_3$  was observed. No measurable isotope effect was observed in the branching behavior of the  $\text{CH}_5^+$  and  $\text{CD}_5^+$  isotopologs although a difference is seen in the 300-K reaction rate coefficients. Possible sources of the discrepancies between reported FALP and CRYRING results has also been discussed.

TABLE V. Measured branching fractions in the DR of  $\text{CD}_5^+$ .

| Channel                               | $\text{CD}_5^{+a}$ | $\text{CH}_5^{+b}$ | $\text{CH}_5^{+c}$ |
|---------------------------------------|--------------------|--------------------|--------------------|
| $\text{CD}_4 + \text{D}$              | 0.059              | 0.049              | 0.95               |
| $\text{CD}_3 + \text{D}_2$            | 0.061              | 0.048              | } $\leq 0.08$      |
| $\text{CD}_3 + 2\text{D}$             | 0.674              | 0.698              |                    |
| $\text{CD}_2 + \text{D}_2 + \text{D}$ | 0.175              | 0.172              | $\leq 0.01$        |
| $\text{CD} + 2\text{D}_2$             | 0.031              | 0.033              | $\leq 0.01$        |

<sup>a</sup>This work (CRYRING).

<sup>b</sup>Semaniak *et al.* [18] (CRYRING).

<sup>c</sup>Molek *et al.* [26] (FALP).

## ACKNOWLEDGMENTS

The authors are grateful to the staff members of Manne Siegbahn Laboratory for technical assistance during the experiment. MK is grateful to the Swedish Institute for the financial support and together with JS acknowledges support by the Ministry of Science and Higher Education, Poland (Grant No. N202 111 31/1194).

- [1] G. A. Olah, R. Klopman, and R. H. Schlosberg, *J. Am. Chem. Soc.* **91**, 3261 (1969).
- [2] E. T. White, J. Tang, and T. Oka, *Science* **284**, 135(1999).
- [3] O. Asvany *et al.*, *Science* **309**, 1219 (2005).
- [4] X. Huang *et al.*, *Science* **311**, 60 (2006).
- [5] Z. Jin, B. J. Braams, and J. M. Bowman, *J. Phys. Chem. A* **110**, 1569 (2006).
- [6] H. Tachikawa and A. J. Orr-Ewing, *J. Phys. Chem. A* **112**, 11575 (2008).
- [7] E. Herbst, *J. Phys. Conf. Series* **4**, 17 (2005).
- [8] E. Herbst, *Astrophys. J.* **222**, 508 (1978).
- [9] S. Green and E. Herbst, *Astrophys. J.* **229**, 121 (1979).
- [10] D. R. Bates, *Astrophys. J.* **306**, L45 (1986).
- [11] T. J. Millar *et al.*, *Astron. Astrophys.* **194**, 250 (1988).
- [12] E. T. Galloway and E. Herbst, *Astrophys. J.* **376**, 531 (1991).
- [13] Å. Larson *et al.*, *Astrophys. J.* **505**, 459 (1998).
- [14] L. Vejby-Christiansen *et al.*, *Astrophys. J.* **483**, 531 (1997).
- [15] S. Kalhori *et al.*, *Astron. Astrophys.* **391**, 1159 (2002).
- [16] A. Ehlerding *et al.*, *Phys. Chem. Chem. Phys.* **6**, 949 (2004).
- [17] A. M. Derkatch *et al.*, *J. Phys. B* **32**, 3391 (1999).
- [18] J. Semaniak *et al.*, *Astrophys. J.* **498**, 886 (1998).
- [19] P. M. Mul *et al.*, *J. Phys. B* **14**, 1353 (1981).
- [20] N. G. Adams, D. Smith, and E. Alge, *J. Chem. Phys.* **81**, 1778 (1984).
- [21] M. Smith and N. Spinel, *Int. J. Mass Spectrom. Ion Processes* **129**, 163 (1993).
- [22] L. Lehfaoui, C. Rebrion-Rowe, S. Laubé, J. B. A. Mitchell, and B. R. Rowe, *J. Chem. Phys.* **106**, 5406 (1997).
- [23] T. Gougousi, M. F. Golde, and R. Johnsen, *Chem. Phys. Lett.* **265**, 399 (1997).
- [24] C. H. Sheehan and J.-P. St. Maurice McLain, *Adv. Space Res.* **33**, 216 (2004).
- [25] J. L. McLain *et al.*, *J. Phys. Chem. A* **108**, 6704 (2004).
- [26] C. D. Molek, V. Poterya, N. G. Adams, and J. L. McLain, *Int. J. Mass Spectrom.* **285**, 1 (2009).
- [27] R. D. Thomas, *Mass Spectrom. Rev.* **27**, 485 (2008).
- [28] T. L. Williams *et al.*, *Mon. Not. R. Astron. Soc.* **282**, 413 (1996).
- [29] S. Datz, G. Sundstrom, C. Biedermann, L. Brostrom, H. Danared, S. Mannervik, J. R. Mowat, and M. Larsson, *Phys. Rev. Lett.* **74**, 896 (1995).
- [30] L. H. Andersen *et al.*, *Phys. Rev. Lett.* **77**, 4891 (1996).
- [31] M. J. Jensen *et al.*, *Astrophys. J.* **543**, 764 (2000).
- [32] V. Zhaunerchyk *et al.*, *Phys. Rev. A* **77**, 034701 (2008).
- [33] L. Viktor *et al.*, *Astron. Astrophys.* **344**, 1027 (1999).
- [34] S. Rosén *et al.*, *Faraday Discuss.* **115**, 295 (2000).
- [35] V. Zhaunerchyk *et al.*, *Mol. Phys.* **103**, 2735 (2005).
- [36] A. Neau *et al.*, *J. Chem. Phys.* **113**, 1762 (2000).
- [37] M. Kaminska *et al.*, *Astrophys. J.* **681**, 1717 (2008).
- [38] J. Öjekull *et al.*, *J. Chem. Phys.* **120**, 7391 (2004).
- [39] R. Thomas *et al.*, *Phys. Rev. A* **66**, 032715 (2002).
- [40] S. Datz *et al.*, *Phys. Rev. Lett.* **85**, 5555 (2000).
- [41] F. Hellberg *et al.*, *J. Chem. Phys.* **122**, 224314 (2005).
- [42] L. Schneider *et al.*, *J. Chem. Phys.* **92**, 7027 (1990).
- [43] P. A. Cook, R. S. Stephen, R. N. Dixon, and M. N. R. Ashfold, *J. Chem. Phys.* **114**, 1672 (2001).
- [44] V. Zhaunerchyk *et al.*, *Phys. Rev. A* **77**, 022704 (2008).
- [45] V. Zhaunerchyk *et al.*, *Phys. Rev. A* **79**, 030701(R) (2009).
- [46] J. R. Peterson *et al.*, *J. Chem. Phys.* **108**, 1978 (1998).
- [47] H. Danared, *Phys. Scr.* **48**, 405 (1993).
- [48] S. Rosén *et al.*, *Phys. Rev. A* **57**, 4462 (1998).
- [49] R. D. Thomas *et al.*, *Phys. Rev. A* **71**, 032711 (2005).
- [50] U. Müller and P. C. Cosby, *Phys. Rev. A* **59**, 3632 (1999).
- [51] A. Hishikawa, H. Hasegawa, and K. Yamanouchi, *Chem. Phys. Lett.* **361**, 245 (2002).
- [52] I. Nevo *et al.*, *Phys. Rev. A* **76**, 022713 (2007).
- [53] V. Zhaunerchyk *et al.*, *J. Chem. Phys.* **130**, 214302 (2009).
- [54] D. Strasser *et al.*, *Phys. Rev. Lett.* **86**, 779 (2001).
- [55] G. Kilgus *et al.*, *Phys. Rev. A* **46**, 5730 (1992).
- [56] A. Paál *et al.*, EPAC Proc. 1, 2748 (2004).
- [57] A. Paál, A. Simonsson, J. Dietrich, and I. Mohos, EPAC Proc. 1, 1196 (2006).
- [58] A. Lampert *et al.*, *Phys. Rev. A* **53**, 1413 (1996).
- [59] J. R. Mowat *et al.*, *Phys. Rev. Lett.* **74**, 50 (1995).
- [60] C. Maul and K.-H. Gericke, *Int. Rev. Phys. Chem.* **16**, 1 (1997).
- [61] E. P. Wigner, *Phys. Rev.* **73**, 1002 (1948).
- [62] J. N. Bardsley, *J. Phys. B* **1**, 365 (1968).
- [63] M. J. Jensen *et al.*, *Phys. Rev. A* **60**, 2970 (1999).
- [64] P. R. Bunker, B. Ostojić, and S. Yurchenko, *J. Mol. Struct.* **695–696**, 253 (2004).
- [65] D. Strasser *et al.*, *Phys. Rev. A* **69**, 064702 (2004).